Indian Journal of Chemistry
Vol. 63, March 2024, pp. 293-303
DOI: 10.56042/ijc.v63i3.6687

New water soluble nickel(II) and copper(II) oxime complexes containing acid group: DNA interaction investigations

Murat Biltekin, Cansu Gökçe Topkaya* & Ramazan Güp

Department of Chemistry, Faculty of Science, Mugla Sıtkı Kocman University, Mugla, Turkey

E-mail: cansutopkaya@mu.edu.tr

Received 10 November 2023; accepted (revised) 23 February 2024

This study explores the DNA-binding and DNA-cleaving properties of two newly synthesized oxime derivative ligands and their complexes with Cu(II) and Ni(II) metal ions. Sodium salts of these compounds have been prepared to ensure water solubility. The structures of the ligands and complexes have been elucidated through various analytical techniques, including ^{1}H NMR, FT-IR, TGA, UV-Vis, SEM-EDS, and XRD analyses. The results reveal that these compounds interact with DNA without significantly altering its structure. They primarily bind to DNA grooves, particularly major grooves. The study has determined that the optimal concentration for these interactions is 75 µM. Viscometry studies show that these compounds do not substantially change DNA viscosity, suggesting groove binding as their mode of interaction without major structural modifications to DNA. Gel electrophoresis, an effective tool for elucidating DNA cleavage mechanisms, indicates that DNA cleavage activity persists in the presence of radical scavengers, although it is reduced, especially in compounds known to bind to DNA grooves. In broader terms, complexes with Ni(II) exhibit higher DNA interaction activity than Cu(II) for both ligands. Among the ligands themselves, H_2L^1 demonstrates higher activity than H_3L^2. In conclusion, this research reveals that these compounds interact with DNA, primarily through groove binding, with minimal impact on DNA structure. This has implications for biomedical and pharmaceutical applications, highlighting these compounds' potential in these fields.

Keywords: Water soluble metal complexes, Oximes, DNA interactions

Transition metal complexes have garnered significant attention from researchers due to their broad applications in fields such as inorganic chemistry, organometallic chemistry, and bioinorganic chemistry[1]. It has been recognized that the presence of metal ions in these complexes can expedite the therapeutic effects and enhance the therapeutic efficacy of the respective organic compounds[2]. The pharmacological activities of metal complexes are intricately linked to the specific metal ions and ligands employed, as different ligands exhibit distinct biological properties[3,4].

In recent years, metal complexes of carboxylic acids and certain derivatives have been successfully employed as model systems in designing novel metallo-pharmaceutical compounds[5]. Carboxylic acid analog compounds are considered one of the most suitable ligand systems for modeling potential pharmacologically active compounds due to their low toxicity, amphiphilic nature, and various biological activities[2,6-7].

Oxime-based ligands and their transition metal complexes have the potential to serve as analytical, spectrophotometric, and bioactive agents[8-10]. However, research on the interactions of these ligands and metal complexes with DNA remains limited[11]. Small molecules of this kind have regained interest in recent years, particularly due to their applicability in various challenging fields such as cancer therapy[12,13], microbial infections[14,15], and molecular biology[16].

In this study, two novel potential bidentate ligands (H_2L^1 and H_3L^2) incorporating both oxime and acid functional groups were synthesized, followed by the preparation of their Cu(II) and Ni(II) complexes. The structures of these compounds were elucidated through a combination of analytical techniques, including ^{1}H NMR, FT-IR, UV-Vis spectroscopy, elemental analysis, thermogravimetric analysis (TGA), X-ray diffraction (XRD), and scanning electron microscopy with energy-dispersive X-ray spectroscopy (SEM-EDS) measurements. Biological activities of the newly synthesized compounds, such as their interactions with DNA binding and DNA cleavage, were examined to elucidate the structure-activity relationships.

Experimental Section

The laboratory materials utilized in this study were commercially sourced from Merck and Sigma. To ensure the purity of the solvents employed for both synthesis and measurements, they underwent meticulous distillation and drying procedures. The pBR322 DNA sample used in the experiments was procured from Fermentas. Microanalysis, encompassing the quantification of carbon (C), nitrogen (N), and hydrogen (H) content, was conducted using a LECO 932 CHNS analyzer. Copper content was determined using atomic absorption spectroscopy on a DV 2000 Perkin Elber ICP-AES instrument Thermo-Scientific Nicolet iS10-ATR IR spectra were obtained using the ATR (attenuated total reflectance) method, covering the spectral range of 4000 to 400 cm^{-1} for solid materials. Magnetic susceptibility assessments were performed at RT on powdered materials using a Sherwood Scientific MK1 Model Gouy Magnetic Susceptibility Balance. Electronic spectra during DNA interaction experiments were recorded with a PG Instruments T80+ UV/Vis Spectrophotometer. Additionally, thermogravimetric analysis was conducted employing a Perkin Elmer Pyris-1 TGA thermal analyzer. Powder X-ray diffraction (XRD) patterns were collected at RT using Cu Ka monochromatic radiation (λ = 1.54056 Å) on a Rigaku-Smart Lab diffractometer. Scanning electron microscopy (SEM) imaging was carried out using a JEOL SEM 7700F instrument, with energy-dispersive X-ray spectroscopy (EDS) analysis performed to assess local composition. The XRD and SEM-EDS investigations were conducted at the Research Centre Laboratory of Muğla Sıtkı Koçman University while ensuring that the results remained distinct and comprehensible without compromising the overall coherence of the information provided. The compound 2-(4-acetylphenoxy)acetic acid was synthesized according to the method described in the litrature[17].

Synthesis of 2-(4-(2-hydroxyimino)acetyl) phenyl) oxy)acetic acid, H_2L^1

The compound was synthesized as follows by modifying the method provided in the patent by McDonough *et al.*[18] A solution of 2-(4-acetylphenoxy)acetic acid (10.31 mmol) was prepared in a mixture of HCl and water (11.54/19.40 mL) at 55°C. Over the course of 3 hours, a solution of sodium nitrite (60.87 mmol) in water (10.45 mL) was added dropwise to this solution. The resulting suspension was then filtered, and hydroxylammonium hydrochloride (92.10 mmol) in solid form was added to the filtrate. The purity of the substance was checked with TLC and the product was purified by crystallization from acetronitrile (Scheme 1). Yield 66%. m.p.194°C. UV-Vis. (H_2O, nm) 230.0, 306.0; FT-IR (ATR): 3500-2900 br (OH), 1729, 1673 s (C=O), 1596 s (C=N), 1242 cm^{-1} m (C-O); ^{1}H NMR (DMSO-d_6): δ 4.83 (s, 2H) (-O*C*H_2), 7.06 (d, 2H), 8.01 (d, 2H) (-Ar*H*), 8.04, (s, 1H) (*H*C=N), 13.17 (s, 1H), 12.41 (s, 1H) (O*H*). Anal. Calcd for $C_{10}H_9NO_5$: C, 53.82; H, 4.06; N, 6.28. Found: C, 53.90; H, 4.10; N, 6.30%.

Synthesis of 2-(4-1,2-bis(hydroxyimino)ethyl) phenoxy)acetic acid, H_3L^2

The compound was synthesized with modifications to the method described in Uysal *et al.*'s 2006 article. Hydroxylammonium hydrochloride (5.38 mmol) and sodium acetate (5.38 mmol) were mixed in an ethanol/water solution. A solution of 2-(4-2-(hydroxyimino)acetyl)phenoxy)acetic acid (H_2L^1) (1.35 mmol) in ethanol was gradually added. The mixture was refluxed for 5 hours, filtered while hot, and the resulting precipitate was left to crystallize. The precipitate was further purified through recrystallization in an H_2O/EtOH mixture (Scheme 2). Yield 58%. m.p.178°C. UV-Vis. (H_2O, nm) 230.0, 278.0; FT-IR (ATR): 3600-2900 br (OH), 1731 s (C=O), 1605 s (C=N), 1234 cm^{-1} m (C-O); ^{1}H NMR (DMSO-d_6): δ 4.65 (s, 2H) (-O*C*H_2), 6.90 (d, 2H), 7.50 (d, 2H) (-Ar*H*), 8.45, (s, 1H) (*H*C=N), 11.5-11.9 (m, 3H) (O*H*). Anal. Calcd for $C_{10}H_{10}N_2O_5$: C, 50.42; H, 4.23; N, 11.76. Found: C, 50.47; H, 4.11; N, 11.75%.

Synthesis of Metal Complexes

The complexes were synthesized as sodium salts in order to enhance their solubility in aqueous solutions

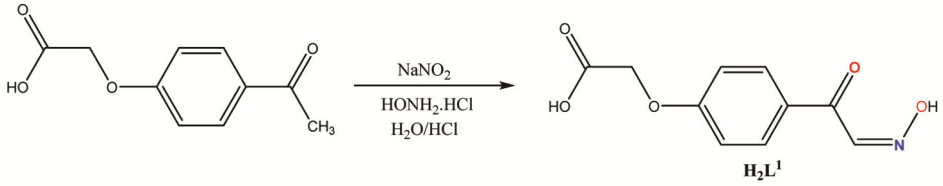

Scheme 1 — Synthesis of acid monoxime ligand (H_2L^1)

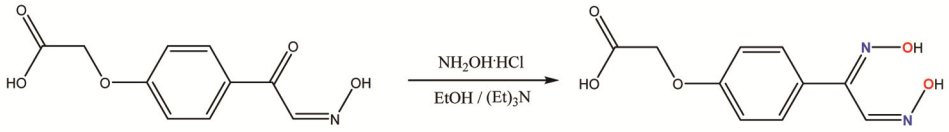

Scheme 2 — Synthesis of acid dioxime ligand (H_3L^2)

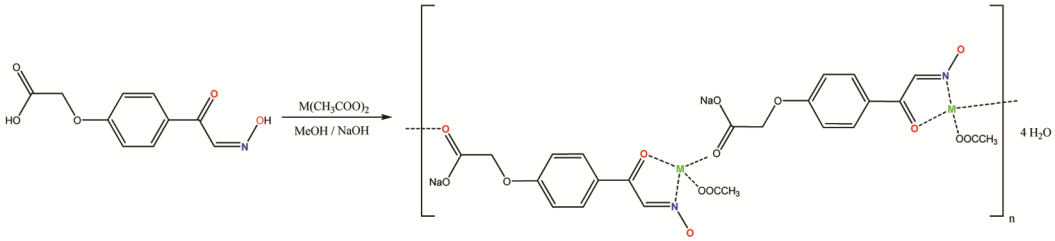

Scheme 3 — Synthesis and proposed structure of metal complexes of H_2L^1 (M: Cu(II) and Ni(II))

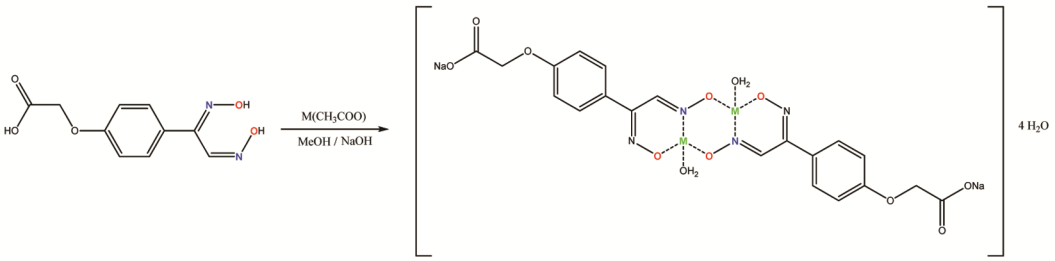

Scheme 4 — Synthesis and proposed structure of metal complexes of H_3L^2 (M: Cu(II) and Ni(II))

due to their lack of solubility in both organic and inorganic solvents. For the synthesis of the complexes, a solution of H_2L^1 and H_3L^2 (1 mmol each) in MeOH was prepared, to which solid NaOH (2 mmol) was added and stirred for 15 minutes. Subsequently, the solutions of metal salts (1 mmol) in MeOH were added to this mixture and stirred under a reflux condenser for 3 hours. The precipitated material was washed with hot EtOH and allowed to crystallize in H_2O afterward (Scheme 3 and Scheme 4).

$[Cu_n(L^1)_n(CH_3COO)_n].2H_2O$: Green complex. Yield 75%. m.p.>350°C. μ_{eff} = 0.72 B.M.; UV-Vis. (DMF, nm) 234.0, 314.0 and 352.0; FT-IR (ATR): 3500-3000 w and br (OH), 1602 m (C=N), 1259 cm^{-1} w (C−O). Anal. Calcd for: C, 35.75; H, 3.50; N, 3.48; Cu, 15.78. Found: C, 35.94; H, 3.03; N, 3.33; Cu, 15.24%.

$[Ni_n(L^1)_n(CH_3COO)_n].2H_2O$: Green complex. Yield 78%. m.p.>350°C. μ_{eff} = 2.04 B.M.; UV-Vis. (DMF, nm) 232.0 and 316.0; FT-IR (ATR): 3500-3000 w and br (OH), 1601 m (C=N), 1252 cm^{-1} w (C−O). Anal. Calcd for: C, 36.22; H, 3.55; N,3.52; Ni, 14.75. Found: C, 36.66; H, 3.62; N, 3.88; Ni, 15.06%.

$[Cu_2(L^2)_2(H_2O)_2].4H_2O$: Brown complex. Yield 70%. m.p.>350°C. μ_{eff} = 1.01 B.M.; UV-Vis. (DMF, nm) 234.0 and 276.0; FT-IR (ATR): 3500-3000 w and br (OH), 1607 m (C=N), 1242 cm^{-1} w (C−O). Anal. Calcd for $C_{20}H_{26}Cu_2N_4Na_2O_{16}$: C, 33.57; H, 3.10; N, 7.83; Cu, 17.76. Found: C, 33.07; H, 3.43; N, 7.65; Cu, 17.14%.

$[Ni_2(L^2)_2(H_2O)_4].2H_2O$: Dark red complex. Yield 74%. m.p.>350°C. μ_{eff} = 1.50 B.M.; UV-Vis. (DMF, nm) 256.0, 298.0 and 406.0; FT-IR (ATR): 3500-3000 w and br (OH), 1607 m (C=N), 1240 cm^{-1} w (C−O). Anal. Calcd for $C_{20}H_{26}N_4Na_2Ni_2O_{16}$:C, 32.28; H, 3.53; N, 7.55; Ni, 15.82. Found: C, 32.17; H, 3.50; N, 7.52; Ni, 15.13%.

Biological studies

DNA binding and DNA cleavage activity studies were carried out by following the procedure reported in our earlier publications[19-21].

Results

Chemistry

In the ^1H NMR spectrum of the H_2L^1 ligand, singlet peaks at 12.41 and 13.17 ppm indicate the

presence of hydroxyl groups, specifically intramolecularly hydrogen-bonded oxime and acidic -OH groups. The hydrogen in the HC=N group of the oxime compound appears as a singlet at 8.01 ppm. In the ^{1}H NMR spectrum of the H_3L^2 ligand, multiplet peaks between 11.5 and 11.9 ppm correspond to hydroxyl groups. The hydrogen within the HC=N group appears as a singlet at 8.01 ppm. Hydrogen atoms on the 1,4-disubstituted benzene ring are observed as a doublet of doublets between 6 and 8 ppm and details given in the experimental section[22-24].

In the IR spectrum of the H_2L^1 ligand, the broad absorption bands observed in the range of 3400-2900 cm^{-1} are attributed to the stretching vibrations (ν(OH)) of hydroxyl groups, indicating their presence. A sharp peak at 1673 cm^{-1} represents the ketone carbonyl (ν(C=O)) bond, while a distinct peak at 1729 cm^{-1} signifies the carboxylic acid carbonyl (ν(C=O)) bond. Additionally, a medium-intensity band at 1596 cm^{-1} corresponds to the ν(C=N) group, providing evidence of a successful oxime reaction. In the IR spectrum of the H_3L^2 ligand, broad peaks in the 3500-2900 cm^{-1} range also correspond to ν(OH) stretching vibrations, indicating the presence of hydroxyl groups. A strong peak at 1731 cm^{-1} is indicative of the carboxylic acid carbonyl (ν(C=O)) bond. Furthermore, medium-intensity peaks at 1605 cm^{-1} are associated with the ν(C=N) group. The disappearance of the ν(C=O) peak at 1673 cm^{-1} suggests the successful completion of the oxime reaction[23,25,26].

The IR spectra of $[Cu(L^1)_n(CH_3COO)_n].2H_2O$ and $[Ni(L^1)_n(CH_3COO)_n].2H_2O$ complexes reveal absorption peaks in the spectral region of 3500-3000 cm^{-1}, which can be attributed to the stretching vibrations (ν(OH)) associated with the crystal water present in these complexes. Notably, the ν(C=O) peak originating from the carboxylic acid group appears weakened and broadened in the range of 1600-1700 cm^{-1}. This effect is primarily due to resonance phenomena occurring between the oxygen atoms at the acidic terminus of sodium and the molecular structure of the ligand, concurrent with the emergence of the ν(C=N) peak. These spectral characteristics align with the structural composition and coordination environments of the complexes. Similarly, in the IR spectra of $[Cu_2(L^2)_2(H_2O)_2].4H_2O$ and $[Ni_2(L^2)_2(H_2O)_4].2H_2O$ complexes, the observed absorption peaks within the 3500-3000 cm^{-1} region correspond to the stretching vibrations (ν(OH)) arising from both crystallographic and coordinated water molecules within the complexes. The ν(C=O) peak, which is linked to the carboxylic acid group and displayed in a manner akin to that in the H_2L^1 ligand complexes, also undergoes weakening and broadening in the range of 1600-1700 cm^{-1}. This outcome stems from resonance interactions between the oxygen atoms at the acidic terminus and the ligand's structural motifs, accompanied by the appearance of the ν(C=N) peak. These spectral manifestations align with the complexes' structural features and coordination environments[23,25].

Peaks observed at approximately 230 nm in the UV-Vis spectra of the ligands are indicative of π→π* transitions associated with the aromatic rings within the compounds. Peaks observed within the range of 300-350 nm are attributed to n→π* electronic transitions. Upon a comparative analysis of the UV-Vis spectra of the complexes and those of the ligands, a notable redshift in the λ_{max} bands of the ligands is observed in the spectra of the complexes. This redshift signifies that the electronic transitions within the complexes have shifted towards longer wavelengths, specifically into the red region of the electromagnetic spectrum, compared to the ligands. The transitions observed in the visible region, typically around ~400 nm, are attributed to charge transfer (CT) transitions occurring within the complexes. These spectral findings align with prior research conducted by other compounds in literature[27,28].

The magnetic moment value of the polymeric structure $[Cu_n(L^1)_n(CH_3COO)_n].2H_2O$ complex is ascertained to be 0.72 B.M. This measurement falls below the typical range (1.72 B.M) observed for compounds containing d^9-configured Cu(II) metal ions. This atypical magnetic moment value is postulated to arise from feeble antiferromagnetic interactions prevailing among the copper(II) ions situated within the molecular framework[27-29]. Similarly, the magnetic moment value for the polymeric structure $[Ni_n(L^1)n(CH_3COO)_n].2H_2O$ complex is determined to be 2.04 B.M, which is notably lower than the magnetic moment values (2.82 B.M) typically associated with d8-configured Ni(II) metal-containing compounds. This diminished magnetic moment value is attributed to the existence of weak antiferromagnetic interactions among the nickel(II) ions present within the molecule[27-29]. The dinuclear complex $[Cu_2(L^2)_2(H_2O)_2].4H_2O$ exhibits a

magnetic moment value of 1.01 B.M, a considerable reduction from the values (3.46 B.M) conventionally witnessed in compounds featuring two d^9-configured Cu(II) metal ions. This peculiar magnetic moment suggests the existence of fragile antiferromagnetic interactions amid the copper(II) ions[30]. Similarly, the dinuclear structure $[Ni_2(L^2)_2(H_2O)_4].2H_2O$ presents a magnetic moment value of 1.50 B.M, which still remains beneath the expected magnetic moment value of 5.64 B.M. This expected value derives from the cumulative contributions of two d^8-configured Ni(II) ions, each possessing two unpaired electrons. The reduced magnetic moment value can similarly be elucidated by positing the existence of subtle antiferromagnetic interactions amid the nickel(II) ions. This phenomenon is commonly observed in polynuclear complexes housing at least two equivalent metal ions, where the spins of the two metal ions align antiparallel to each other[27,28,31].

Both the $[Cu_n(L^1)_n(CH_3COO)_n].2H_2O$ and $[Ni_n(L^1)_n(CH_3COO)_n].2H_2O$ complexes undergo a three-stage thermal gravimetric decomposition process. The initial stage, transpiring within the temperature range of 55-120°C, results in a mass loss of approximately 9.00% (9.80%) and is attributed to the expulsion of two moles of crystal water, which were not involved in coordination. The subsequent stage, spanning from 120-200°C, involves a mass loss of around 7.00% (7.18%) and is presumed to signify the detachment of one mole of acetate group, believed to be part of the coordination sphere. The ultimate stage involves the complete degradation of the ligand, leaving metal oxides as the final residue. In a similar manner, the $[Cu_2(L^2)_2(H_2O)_2].4H_2O$ complex exhibits a three-stage thermal gravimetric decomposition process. The initial stage, manifesting between 55-120°C, results in a mass loss of approximately 10.00% (10.30%), entailing the removal of four moles of crystal water not involved in coordination. The subsequent stage, occurring in the temperature range of 120-250°C, leads to a mass loss of about 20.00% (19.60%). During this stage, it is postulated that two moles of H_2O group, presumed to be part of the coordination environment, are detached from the structure, and the ligand initiates degradation. The final stage corresponds to the complete decomposition of the ligand, yielding copper oxides as the residual product. In the case of the $[Ni_2(L^2)_2(H_2O)_4].2H_2O$ complex, a three-stage thermal gravimetric decomposition process is similarly observed. The initial stage, occurring within the temperature range of 55-120°C, leads to a mass loss of approximately 5.00% (5.20%), involving the removal of two moles of crystal water not coordinated to the complex. The subsequent stage, spanning 120-200°C, results in a mass loss of around 10.00% (9.60%) and is believed to entail the detachment of four moles of H_2O group, presumed to be part of the coordination sphere. The ultimate stage involves the complete degradation of the ligand, leaving nickel oxides as the final residue. These thermal decomposition profiles provide valuable insights into the complexes' stability and behavior across varying temperature ranges.

The powder X-ray diffraction studies of the complex compounds were carried out at RT using CuK_α monochromatic radiation with a wavelength (λ) of 1.54056 Å. The analysis of the spectra reveals that the complexes $[Cu_n(L^1)_n(CH_3COO)_n].2H_2O$, $[Cu_2(L^2)_2(H_2O)_2].4H_2O$, and $[Ni_2(L^2)_2(H_2O)_4].2H_2O$ exist in an amorphous state due to the broad peaks observed in their spectra. In contrast, for the complex $[Ni_n(L^1)_n(CH_3COO)_n].2H_2O$, the presence of sharp peaks alongside broad peaks suggests that this complex coexists in both amorphous and crystalline states[23,32].

The SEM micrographs of the complexes were obtained using a scanning electron microscope under an accelerated voltage of 15 kV and at magnification ratios ranging from 100x to 250x (Fig. 1). To determine the presence of metal in the complexes' structures, energy-dispersive spectroscopy (EDS) was

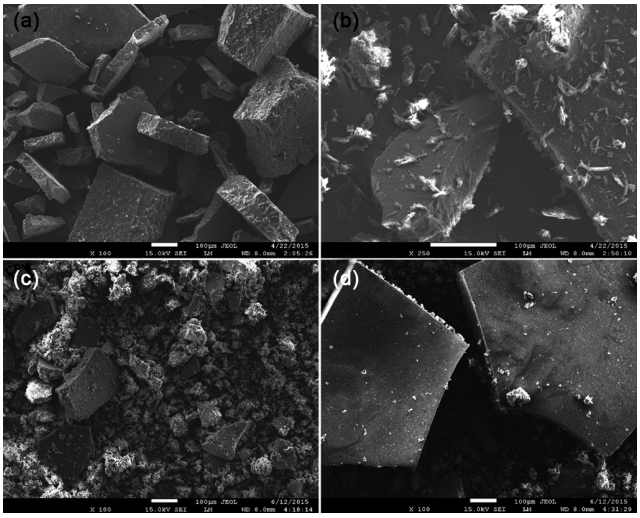

Fig. 1 — The SEM images of the compounds (a) $[Cu_n(L^1)_n(CH_3COO)_n].2H_2O$ (b) $[Ni_n(L^1)_n(CH_3COO)_n].2H_2O$ (c) $[Cu_2(L^2)_2(H_2O)_2].4H_2O$ (d) $[Ni_2(L^2)_2(H_2O)_4].2H_2O$

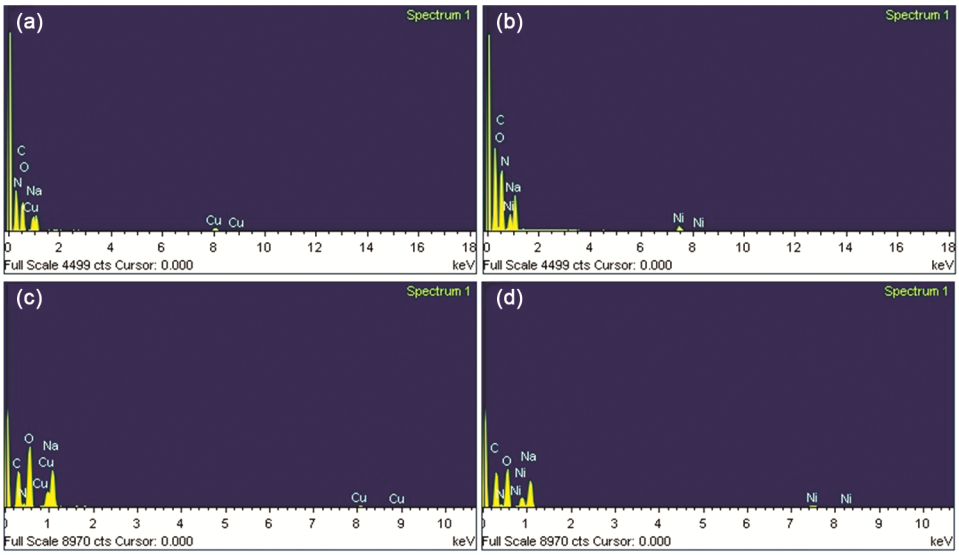

Fig. 2 — The energy-dispersive spectras of the compounds (a) $[Cu_n(L^1)_n(CH_3COO)_n].2H_2O$ (b) $[Ni_n(L^1)_n(CH_3COO)_n].2H_2O$ (c) $[Cu_2(L^2)_2(H_2O)_2].4H_2O$ (d) $[Ni_2(L^2)_2(H_2O)_4].2H_2O$

employed. Analysis of the data from the EDS spectra revealed that the structures of $[Cu_n(L^1)_n(CH_3COO)_n].2H_2O$ and $[Cu_2(L^2)_2(H_2O)_2].4H_2O$ complexes exclusively contained C, N, O, Na, and Cu atoms, while $[Ni_n(L^1)_n(CH_3COO)_n].2H_2O$ and $[Ni_2(L^2)_2(H_2O)_4].2H_2O$ complexes exclusively comprised C, N, O, Na, and Ni atoms (Fig. 2). EDS spectra confirm the formation of complexes and the presence of Na ions in the structures[28,32].

DNA Binding

The UV-vis spectroscopic analysis of ligands and complexes was conducted to investigate their DNA binding activities. The results, including Δλ (wavelength difference), %H (hypochromism), and K_b (binding constant), are presented in Table 1. In the case of H_2L^1 compound, the interaction with CT-DNA revealed a hypochromic shift of 2 nm from 306 nm to 304 nm, along with a decrease in absorbance (hypochromism) at 306 nm, as DNA concentration increased (Fig. 3). The isobestic point indicating ligand/complex-DNA complex formation was observed at 298 nm. For H_3L^2 compound, the interaction with CT-DNA showed hyperchromism with an increase in absorbance at 230 nm, and a hypochromic shift of 2 nm to 228 nm as DNA concentration increased. In the case of $[Cu_n(L^1)_n(CH_3COO)_n].2H_2O$, a hypochromic shift of 4 nm from 352 nm to 348 nm was observed, along with a decrease in absorbance at 352 nm, as DNA concentration increased. The isobestic point indicating ligand/complex-DNA complex formation was observed at 311 nm. For $[Ni_n(L^1)_n(CH_3COO)_n].2H_2O$, a hypochromic shift of 8 nm from 316 nm to 308 nm was observed, along with a decrease in absorbance at 316 nm, as DNA concentration increased. The isobestic point indicating ligand/complex-DNA complex formation was observed at 309 nm. In the case of $[Cu_2(L^2)_2(H_2O)_2].4H_2O$, hyperchromism was observed with an increase in absorbance at 234 nm, and a hypochromic shift of 2 nm to 232 nm as DNA concentration increased. Additionally, an isobestic point was observed at 294 nm. For $[Ni_2(L^2)_2(H_2O)_4].2H_2O$, hyperchromism was observed with an increase in absorbance at 256 nm, and a hypochromic shift of 6 nm to 250 nm as DNA concentration increased. Additionally, an isobestic point was observed at 289 nm. The UV-vis spectroscopic analysis of the synthesized compounds revealed that their spectra exhibited minor changes upon DNA binding, indicating a binding mode that

Table 1 — CT-DNA binding results of synthesized compounds

Compd	Δλ (nm)	H (%)	Kb (M^{-1})
H_2L^1	2 (blue shift)	3,7	$3,00\times10^3$
H_3L^2	2 (blue shift)	–16,17	$6,67\times10^2$
$[Cu_n(L^1)_n(CH_3COO)_n].2H_2O$	4 (blue shift)	30	$8,00\times10^3$
$[Ni_n(L^1)_n(CH_3COO)_n].2H_2O$	8 (blue shift)	1,95	$9,57\times10^3$
$[Cu_2(L^2)_2(H_2O)_2].4H_2O$	2 (blue shift)	–21,31	$2,50\times10^3$
$[Ni_2(L^2)_2(H_2O)_4].2H_2O$	6 (blue shift)	–23,73	$5,00\times10^3$

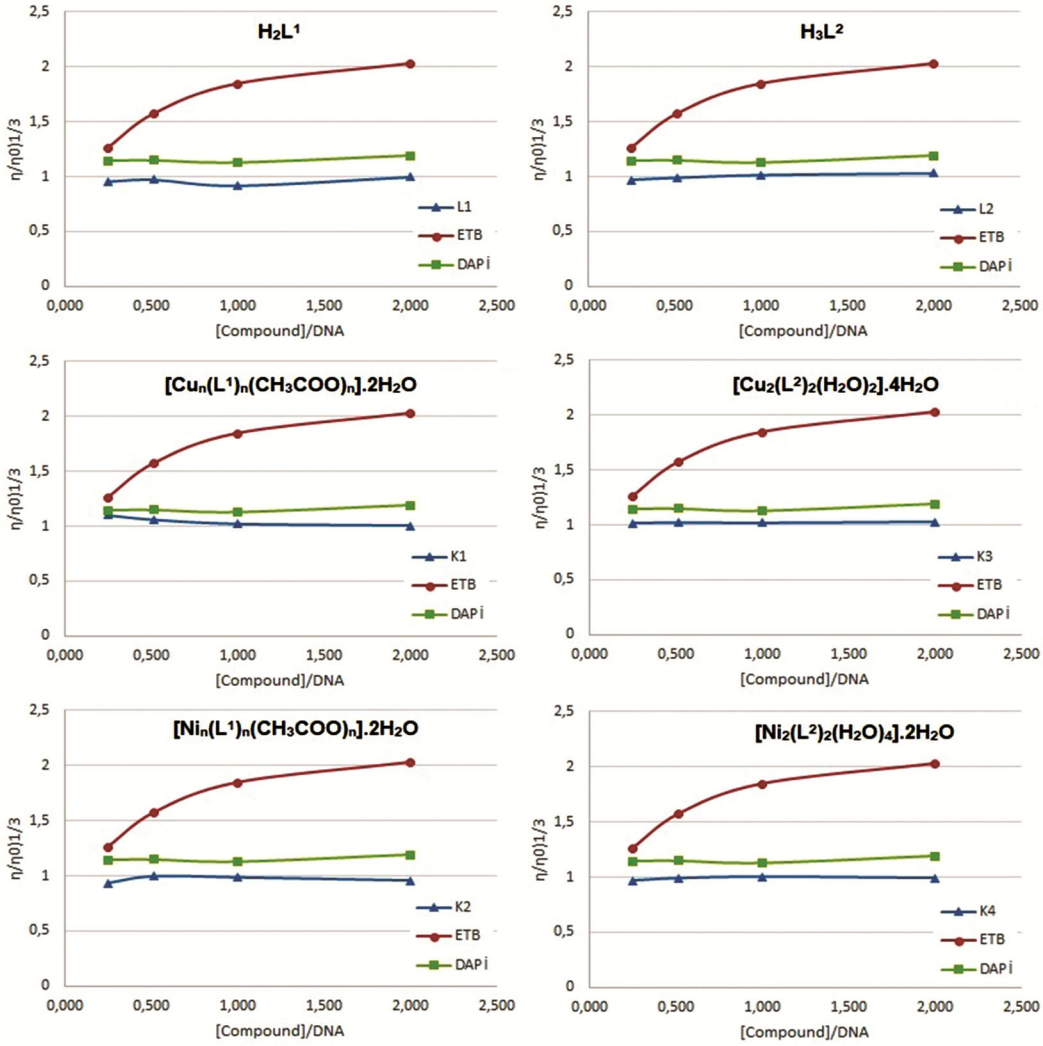

Fig. 3 — CT-DNA binding results obtained by viscosity measurement of compounds

does not significantly disrupt the DNA helical structure, possibly involving binding to grooves or electrostatic interactions[21,33,34].

The results of the studies conducted using viscometry for the compounds were compared with compounds known for their strong intercalation properties, ethidium bromide (EB), and compounds known to bind to grooves, such as DAPI (4',6-diamidino-2-phenylindole). The obtained results indicated that the viscosities of all compounds were similar to DAPI, which is known to bind to grooves. In the study involving length change-sensitive hydrodynamic measurements, no increase in viscosities was observed for all ligands and complexes.

These results are consistent with the binding mode of compounds, which may involve binding to grooves without significantly disrupting the conformation of DNA. This observation, when combined with the results from UV-vis spectroscopy, suggests that the compounds bind to DNA in a manner that does not heavily distort its conformation[34,35].

DNA Cleavage

In the experiments conducted to determine the optimum ligand/complex concentration for the compounds, it was observed that as the compound concentration increased, the cleavage activity increased, accompanied by an increase in Form II and Form III, and a decrease in Form I quantities (Fig. 4). Based on these results, the optimum concentration for all compounds in both oxidative and hydrolytic studies was determined to be 75 µM (Fig. 5).

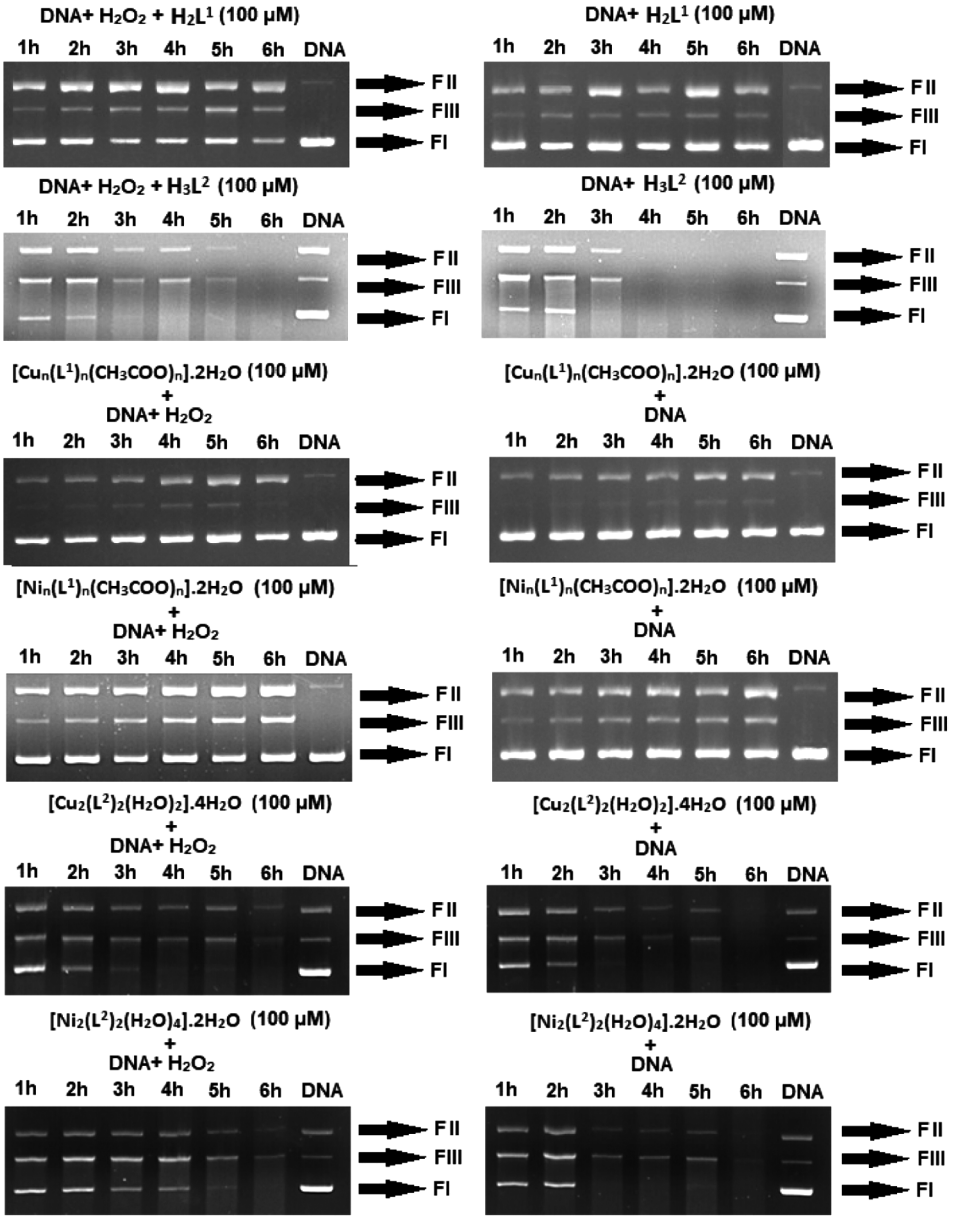

Fig. 4 — DNA cleavage activities of compounds dependent on incubation time (1-6 h) under oxidative and hydrolytic conditions

Furthermore, gel electrophoresis is an effective method used to determine the active species in cleavage reactions. Therefore, hydrolytic and oxidative DNA cleavage reactions were investigated in competition with various radical scavengers (superoxide radical ($\bullet O_2^-$) scavenged by superoxide dismutase (SOD), hydrogen peroxide scavenged by catalase, $^1O_2$ radical scavenged by NaN_3, OH• radical scavenged by DMSO and KI, minor groove binder Methyl Green, and major groove binder DAPI) to determine the binding mode[21,36,37] (Fig. 6).

In the cleavage mechanism studies conducted for H_2L^1 ligand, it is understood that the radicals we examined in the cleavage mechanism were not effective, as the addition of radical scavengers did not stop the cleavage activity. In the mechanism studies, it is observed that cleavage is reduced only in the presence of competitive binding to DNA grooves, especially the major groove, as indicated by an increase in uncleaved DNA (Form I) and a decrease in double-stranded cleaved DNA (Form III). This suggests that the ligand primarily binds to the DNA grooves, especially the major groove, to facilitate cleavage.

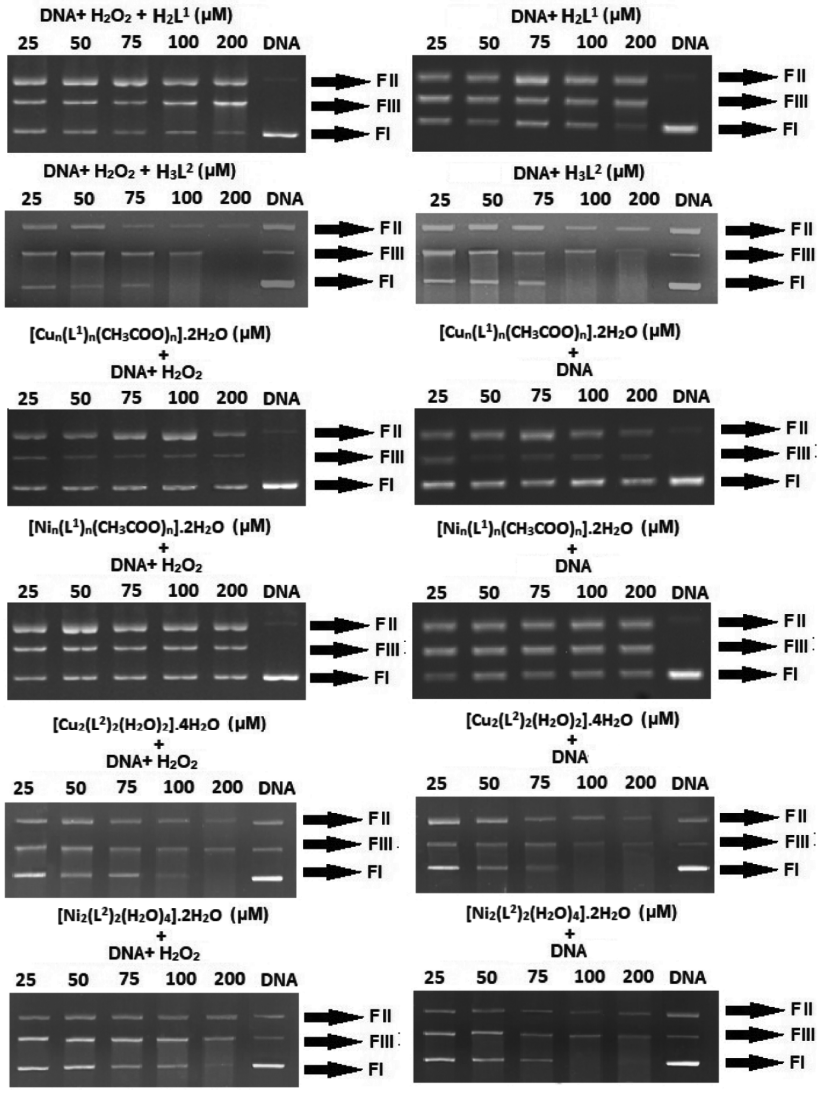

Fig. 5 — Concentration-dependent DNA cleavage activities of complexes under oxidative and hydrolytic conditions (25-200 μM)

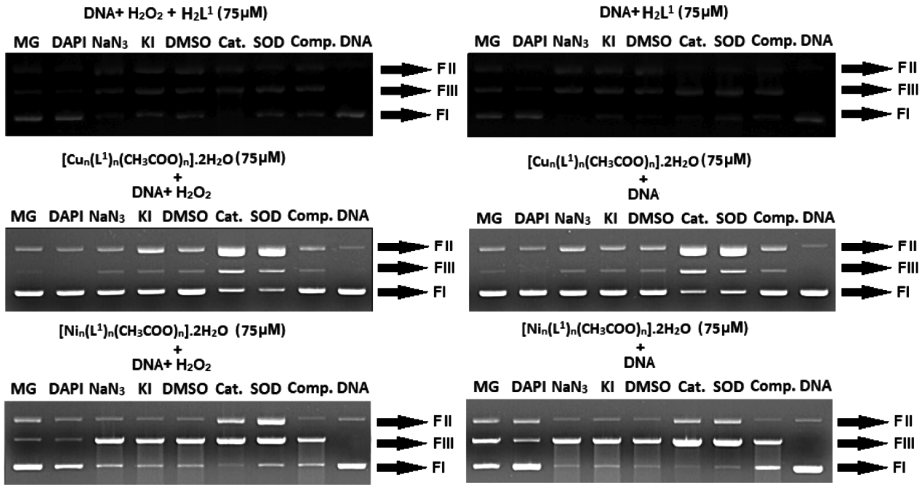

Fig. 6 — The DNA cleavage mechanism of selected compounds under hydrolytic (A) and oxidative (B) conditions

In the cleavage mechanism determination studies for $[Cu_n(L^1)_n(CH_3COO)_n].2H_2O$ complex, it is observed that cleavage completely ceases in the presence of DAPI, and there is a significant reduction in double-stranded cleavage in the presence of Methyl Green. Additionally, the results indicate that the studied radical scavengers do not affect the cleavage mechanism. This implies that the complex primarily binds to DNA grooves, especially the major groove, to facilitate cleavage. In the cleavage mechanism determination studies for $[Ni_n(L^1)_n(CH_3COO)_n].2H_2O$ complex, it is understood that the cleavage activity decreases in the presence of both DAPI and Methyl Green, as indicated by an increase in uncleaved DNA (Form I). Additionally, the results show that the used radical scavengers do not affect the cleavage mechanism. This suggests that $[Ni_n(L^1)_n(CH_3COO)_n].2H_2O$ complex primarily binds to DNA grooves, especially the major groove, to facilitate cleavage.

Discussion

Within the scope of this study, two novel oxime derivative ligands were synthesized, and their complexes with Cu(II) and Ni(II) metal ions were prepared. The sodium salts of these ligands and complexes were obtained to ensure their solubility in water. The structures of the synthesized ligands and complexes were elucidated through various analytical techniques, including ^{1}H NMR, FT-IR, TGA, UV-vis, SEM-EDS, and XRD analyses.

The elucidated structures of the synthesized ligands and complexes enabled the investigation of their DNA-binding and DNA-cleaving activities. The DNA-binding and DNA-cleaving activities of these artificial nucleases were studied using UV-Vis titration, viscometry, and gel electrophoresis methods with CT-DNA and plasmid pBR322.

This study aimed to provide insights into the structures and activities of the newly synthesized compounds in the context of DNA interactions and cleavage mechanisms.

The results of UV-vis spectroscopy indicate that the interactions of the compounds with DNA minimally affect the structure of DNA. These interactions primarily occur through binding to DNA grooves, particularly the major grooves. Furthermore, it was determined that the optimal concentration of the compounds is 75 μM.

Viscometry studies reveal that the examined compounds do not cause a significant increase in DNA viscosity, suggesting that they interact with DNA by binding to grooves without extensively altering DNA structure.

The gel electrophoresis results, which are an effective method for determining DNA cleavage mechanisms, indicate that the DNA cleavage activity of the compounds continues in the presence of various radical scavengers. However, this activity is notably reduced, particularly in compounds known to bind to DNA grooves.

If we categorize the DNA interaction activities of the complexes based on the respective metals they contain, it is evident that for both ligands, Ni(II) exhibits a higher level of activity compared to Cu(II). Additionally, when considering the ligands themselves, the order of activity is established as $H_2L^1 > H_3L^2$.

In conclusion, this research examined the interactions of different ligand and complex compounds with DNA, demonstrating that these interactions minimally affect DNA structure while primarily involving binding to grooves, notably the major grooves. These findings suggest the potential candidacy of these compounds for biomedical and pharmaceutical applications.

Supplementary Information

Supplementary information is available in the website http://nopr.niscpr.res.in/handle/123456789/58776.

References

1 Boerner L J & Zaleski J M, *Curr Opin Chem Biol*, 9 (2005) 135.
2 Siddiqi Z A, Khalid M, Kumar S, Shahid M & Noor S, *Eur J Med Chem,* 45 (2010) 264.
3 Delaney S, Pascaly M, Bhattacharya P K, Han K & Barton J K, *Inorg Chem*, 41 (2002) 1966.
4 Çolak A, Terzi Ü, Çol M, Karaoğlu Ş A, Karaböcek S, Küçükdumlu A & Ayaz F A, *Eur J Med Chem*, 45 (2010) 5169.
5 Sakurai H, Kojima Y, Yoshikawa Y, Kawabe K & Yasui H, *Coord Chem Rev*, 226 (2002) 187.
6 González-Baró A C, Castellano E E, Piro O E, Parajón-Costa B S, *Polyhedron* 24 (2005) 49.
7 Setlow B & Setlow P, *Appl Environ Microbiol*, 59 (1993) 3418.
8 Topkaya C G, Çetin E S, Göktürk T, Kincal S, Hökelek T & Gup R, *Inorg Chem Commun*, 155 (2023) 111040.
9 Singh R B, Garg B S & Singh R P, *Talanta*, 26 (1979) 425.
10 Georgieva I, Trendafilova N & Bauer G, *Spectrochim Acta A Mol Biomol Spect,* 63 (2006) 403.
11 Babu M S, Reddy K H & Krishna P G, *Polyhedron*, 26 (2007) 572.
12 Kelland L R, *Eur J Cancer*, 41 (2005) 971.

13 Mukherjee S, Chowdhury S, Ghorai A, Ghosh U & Stoeckli-Evans H, *Polyhedron*, 51 (2013) 228.
14 Otero L, Marisol V, Lucia B, Ana D, Carolina R, Lucia O, Olea A C, Diego M J, Antonio M, Krauth S R L, Piro O E, Ernesto C E, Mercedes G, Dinorah G & Hugo C, *J Med Chem*, 49 (2006) 3322.
15 Bandyopadhyay N, Zhu M, Lu L, Mitra D, Das M, Das P, Samanta A & Naskar J P, *Eur J Med Chem*, 89 (2015) 59
16 Bandyopadhyay N, Pradhan AB, Das S, Lu L, Zhu M, Chowdhury S & Naska J P, *J Photochem Photobiol B*, 160 (2016) 336
17 Kumar Y, Gowrishankar R, Aryan R C, Bhushan K H & Mishra M K, *Patent No. WO2004089945A1*, 2004. (https://patents.google.com/patent/WO2004089945A1/en?oq=WO2004089945A1).
18 McDonough J A, Tafesh A M & Fruchey O S, *US Patent No. US005319142A*, 1994.
19 Gokce C & Gup R, *Chem Pap*, 67 (2013) 1293.
20 Topkaya C G, Göktürk T, Hökelek T, Çetin E S, Kincal S & Güp R, *J Mol Struct*, 1266 (2022) 133453.
21 Göktürk T, Topkaya C, Sakallı Çetin E & Güp R, *Chem Pap*, 76 (2022) 2093.
22 Acker F A V, Hageman J A, Haenen G R, Vijgh W J V D, Bast A & Menge W M, *J Med Chem*, 43 (2000) 3752.
23 Güp R, Gökçe C & Dilek N, *J Photochem Photobiol B*, 144 (2015) 42.
24 Gup R, Gökçe C & Dilek N, *Supramol Chem*, 27 (2015) 629.
25 Koning M C D, Grol M V & Noort D, *Toxicol Lett*, 206 (2011) 54.
26 Topkaya C, Aslan S, Hökelek T, Göktürk T, Kıncal S, Altuntaş D B & Güp R, *J Mol Struct*, 1265 (2022) 133339.
27 Güp R & Kırkan B, *Spectrochim Acta Part A Mol Biomol Spect*, 62 (2005) 1188.
28 Güp R & Kırkan B, *Spectrochim Acta A Mol Biomol Spect*, 64 (2006) 809.
29 Coşkun A & Karataş İ, *Turk J Chem*, 28 (2004) 173.
30 Tumer M, Ekinci D, Tumer F & Bulut A, *Spectrochim Acta Part A Mol Biomol Spect*, 67 (2007) 916.
31 Ivanovic-Burmazovic I, Bacchi A, Pelizzi G & Leovac V M, *Polyhedron*, 18 (1998) 119.
32 Gökçe C & Güp R, *J Photochem Photobiol B*, 122 (2013) 15.
33 Sirajuddin M, Ali S & Badshah A, *J Photochem Photobiol B*, 124 (2013) 1.
34 Şengül E E, Göktürk T, Topkaya C G & Gup R, *J Chil Chem Soc*, 65 (2020) 4754.
35 Zhang S, Sun X, Qu F & Kong R, *Spectrochim Acta A Mol Biomol Spect*, 112 (2013) 78.
36 Trotta E, Grosso N D, Erba M & Paci M, *Biochem*, 39 (2000) 6799.
37 Dong X, Wang X, Lin M, Sun H, Yang X & Guo Z, *Inorg Chem*, 49 (2010) 2541.